AGU PUBLICATIONS

JGR

Journal of Geophysical Research: Atmospheres

RESEARCH ARTICLE
10.1002/2017JD027637

Key Points:
- A Bayesian retrieval scheme is developed for vertical velocity, latent heating, and hydrometeor water contents
- Experiments assimilating the three variables were able to improve the analysis as well as the forecast track
- Latent heating and hydrometeors have similar positive impacts on the assimilation

Correspondence to:
Y. Lee,
ylee@atmos.colostate.edu

Citation:
Lee, Y., Kummerow, C. D., & Zupanski, M. (2018). Impacts of assimilating vertical velocity, latent heating, or hydrometeor water contents retrieved from a single reflectivity data set. *Journal of Geophysical Research: Atmospheres*, *123*, 1673–1693. https://doi.org/10.1002/2017JD027637

Received 21 AUG 2017
Accepted 12 DEC 2017
Accepted article online 18 DEC 2017
Published online 3 FEB 2018

Impacts of Assimilating Vertical Velocity, Latent Heating, or Hydrometeor Water Contents Retrieved From a Single Reflectivity Data Set

Yoonjin Lee[1], Christian D. Kummerow[1], and Milija Zupanski[2]

[1]Department of Atmospheric Science, Colorado State University, Fort Collins, CO, USA, [2]Cooperative Institute for Research in the Atmosphere, Colorado State University, Fort Collins, CO, USA

Abstract Assimilation of observation data in cloudy regions has been challenging due to the unknown properties of clouds such as cloud depth or cloud drop size distributions (DSD). Attempts to assimilate data in cloudy regions generally assume a DSD, but most assimilation systems fail to maintain consistency between models and the observation data, as each has its own set of assumptions. This study tries to retain the consistency between the forecast model and the retrieved data by developing a Bayesian retrieval scheme that uses the forecast model itself for the a priori database. Through the retrieval algorithm, vertical profiles of three variables related to the development of tropical cyclones, including vertical velocity (VV), latent heating (LH), and hydrometeor water contents (HYDRO), are derived from the same reflectivity observation. Each retrieved variable is assimilated in the data assimilation system using a flow-dependent forecast error covariance matrix. The simulations are compared to evaluate the respective impact of each variable in the assimilation system. In this study, three assimilation experiments were conducted for two hurricane cases captured by the Global Precipitation Measurement satellite: Hurricane Pali (2016) and Hurricane Jimena (2015). Analyses from these two hurricane cases suggest that assimilating LH and HYDRO have similar impacts on the assimilation system while VV has less of an impact than the other two variables. Using these analyses as an initial condition for the forecast model reveals that the assimilations of retrieved LH and HYDRO were able to improve the track forecast as well.

1. Introduction

The importance of the initial condition is indisputable in a prediction of nonlinear weather systems (Kalnay, 2003). Weather forecast models, being themselves imperfect, depend critically on the initial conditions provided to the model. The most efficient and mathematically consistent way of improving initial conditions for numerical weather prediction models is data assimilation (DA) using observations that are available around the world (Zupanski, 1993). DA blends information from the observations and the forecast model based on Bayes' theorem and produces an optimized initial condition. Both new observations and DA techniques have contributed to improvements in forecasting skill (Kalnay, 2003). Satellite data are one of the most important observations assimilated in atmospheric data assimilation, due to their geographical coverage and information content. Satellite data in clear-sky regions have been preferred for assimilation over cloudy-sky data due to the simplification of not having to specify uncertain cloud properties in the radiative transfer model (RTM) (S. Q. Zhang et al., 2013). However, it is not the most effective way to use the vast amount of available satellite data for cloudy regions where conditions can change rapidly and detailed forecasts are often critical (Wu & Zupanski, 2017). When it comes to hurricane simulations, clear-sky assimilation schemes can make little or no use of dedicated satellites such as the Tropical Rainfall Measuring Mission (TRMM) and its successor, the Global Precipitation Measurement (GPM), because there are few clear regions. In order to make the best use of these data, the DA community is therefore slowly moving toward cloudy-sky DA, even though it is far more complex than clear-sky DA (M. Zhang et al., 2013).

Clear-sky DA is mostly conducted with raw radiances due to their well-defined observation errors (Derber & Wu, 1998; Ma et al., 2017; Okamoto & Derber, 2006). Observation errors from uncertainties in the RTM are relatively small without introducing a cloud. However, once thick clouds or precipitation enter a scene, observation errors grow significantly due to subgrid-scale cloud variability as well as cloud and precipitating particle size distribution for a calculation of scattering properties (Errico et al., 2007). Moreover, larger

dynamic ranges of the brightness temperature (T_b) with the existence of clouds make the observation error of the cloudy-sky radiance even larger (Geer & Bauer, 2010). Nevertheless, cloud-affected radiances are assimilated more frequently in the forecast model these days because, despite large uncertainties, their information is still valuable, especially in a precipitating situation (M. Zhang et al., 2013; Zhu et al., 2016). Although cloudy-sky radiance assimilation shows a clear improvement on the forecast (Geer et al., 2010; Yang et al., 2016; M. Zhang et al., 2013), radiances are not the only variables that can be assimilated. Some studies showed improvements in forecasting skill after assimilation of cloud liquid/ice water path (Chen et al., 2015; Wu et al., 2016) or cloud optical depth (Benedetti & Janisková, 2008).

Vertical profiles of liquid water and ice can be retrieved from ground-based radar reflectivity. Radar products are operationally used in the High-Resolution Rapid Refresh (HRRR) model. Radar reflectivity is used to create a cloud analysis in the HRRR model, but it is also assimilated as a form of temperature tendency or latent heating (LH) to control the model dynamics in the initial time step (Benjamin et al., 2016). With the adjusted temperature tendency, it can trigger convection or subsidence in the right place of the system. Such dynamical variables that are related to convection of the system such as vertical velocity (VV) or LH can be beneficial when the model dynamics need to be adjusted in the initial condition.

Over vast oceanic regions, only satellite data are available. Retrievals from satellite observed radiances or reflectivities can produce multiple variables related to clouds, and sometimes the same observation can provide multiple products. The Goddard profiling algorithm (GPROF) produces vertical structures of hydrometeor as well as LH from passive microwave observations using a Bayesian approach (Olson et al., 1999). Although its products are valuable, they have not been assimilated because a new observation operator for the products had to be developed. Recently, Wu et al. (2016) developed a new observation operator for the Hurricane Weather Research and Forecast system in Gridpoint Statistical Interpolation to provide an ability to assimilate hydrometeor water contents (HYDRO) outputs from GPROF.

Here we seek the optimal variables derived from spaceborne radars aboard the GPM spacecraft (Hou et al., 2014) for DA application. A simple retrieval of VV, LH, and HYDRO was developed for this study. For the retrieval, an a priori database was created with the Weather Research and Forecast (WRF) model, which is also used in the DA experiments, and vertical profiles of the three variables are stored along with the computed reflectivity profile. The retrieval simply finds the best matching reflectivity profile from the database. Using an a priori database is a very common process in retrieving cloud parameters from the satellite observation because it is an underconstrained problem (Kummerow et al., 2015). By using the WRF model both as a forecast model in the DA system and as an a priori, the retrieved products are thus kept consistent with the microphysical scheme in the forecast model. This is promising because most assimilation systems fail to maintain consistency between models and the observation data, as each has its own set of assumptions.

This study provides a direct experiment of the impact of assimilating three different variables into WRF, although all three variables are derived from the same reflectivity profile. Given an ability to retrieve HYDRO as well as LH and VV, this study will explore the impact of assimilating each of the three different variables derived from the same radar reflectivity observations to assess their respective impact on the DA system. As a DA system, an ensemble method is used to benefit from a flow-dependent forecast error covariance since a static error covariance is not appropriate for hurricanes. The three DA experiments were conducted for two hurricane cases (Hurricane Pali (2016) and Jimena (2015)), and each result is presented in section 4.

2. Retrieval Algorithm

Vertical profiles of cloud-related variables can be retrieved from a space borne radar through optimal estimation. Unlike Bayesian schemes**,** which require a priori data to retrieve variables, its vertical information allows the retrieval to be done without any a priori information. Thus, although the operational radar algorithm for GPM does not require any a priori, variables are retrieved using ancillary environmental data and assumptions in the drop size distribution (DSD) (Iguchi et al., 2010). According to the GPM/dual-frequency precipitation radar (DPR) Level-2 Algorithm Theoretical Basis Document (Iguchi et al., 2010), single-frequency radar such as the precipitation radar (PR) on TRMM has to assume a size distribution with a single parameter due to insufficient number of measurements and this can lead to significant retrieval errors. With the additional frequency channel such as in dual-frequency precipitation radar on the GPM satellite, two parameters in the DSD can be retrieved as well as the precipitation rate. It is convenient to use reflectivity to retrieve

Table 1
Table for WRF Physics

Microphysics	Modified WDM6 scheme
Long wave radiation physics	RRTM scheme
Short wave radiation physics	MM5 shortwave scheme
Cumulus parameterization	New Kain-Fritsch scheme
Land surface model	Noah land surface model
Surface layer	Monin-Obukhov similarity theory
Planetary boundary layer	YSU PBL scheme

those variables since reflectivity can be expressed as a function of DSD and there is a direct relationship between reflectivity and precipitation rate. However, other variables such as LH or VV that are indirectly related to clouds, but not detected by radar, cannot be retrieved solely from reflectivity due to the lack of a direct linkage, and Bayesian methods are generally needed. Additional information such as rainfall system type (convective or stratiform) is required as well as reflectivity to better constrain the grid dynamics during the retrieval, which will be discussed later. Since LH and VV cannot be observed, numerical models are the only way to provide information about these variables. Therefore, this study uses a forecast model to produce an a priori database that contains possible combinations of VV, LH, and HYDRO that correspond to a certain reflectivity profile. The WRF model, which is used in both the a priori database creation and the DA experiments, does not produce reflectivity with the WRF Double-Moment 6 class microphysical (WDM6) (Lim & Hong, 2010) scheme. The Eddington model (Kummerow, 1993) was then coupled with the WRF outputs to produce simulated reflectivities.

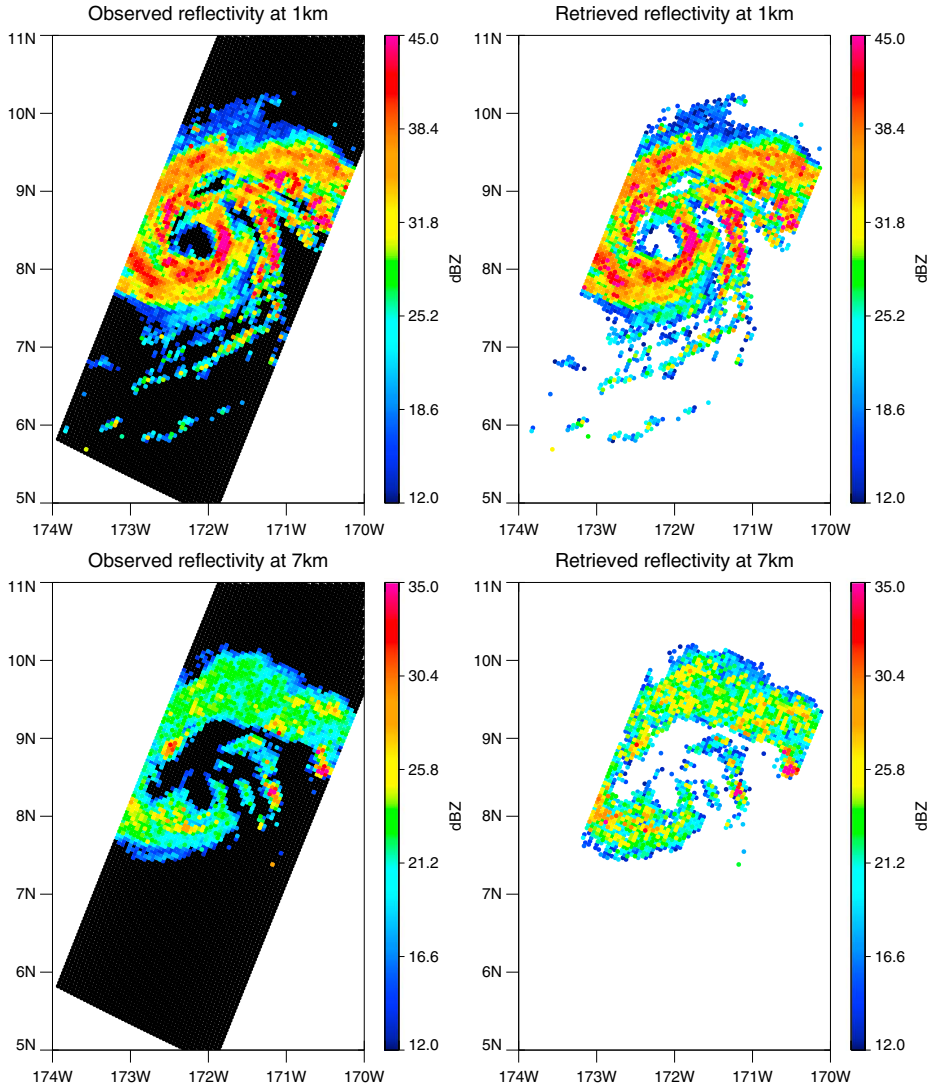

Figure 1. (left) Observed and (right) retrieved reflectivity horizontal cross section at (top) 1 km and (bottom) 7 km for Hurricane Pali (2016).

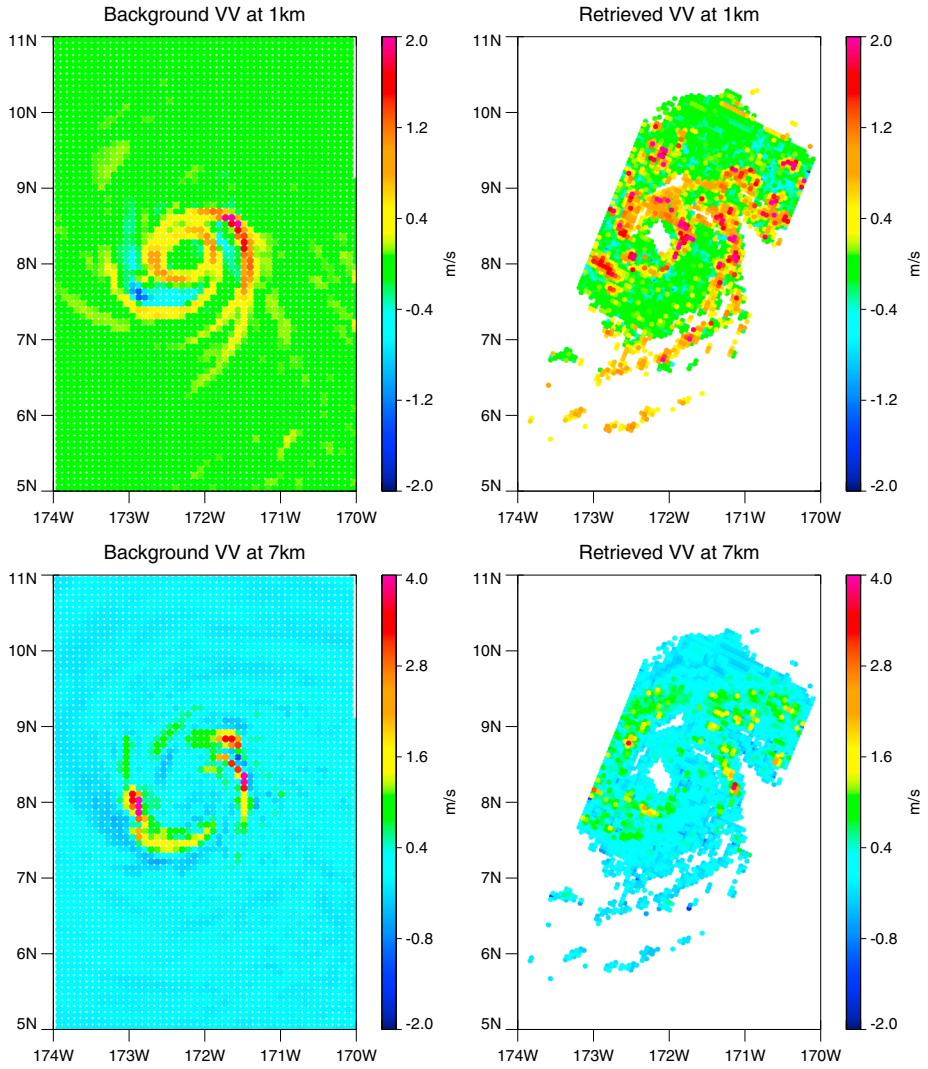

Figure 2. (left) Background and (right) retrieved vertical velocity horizontal cross section at (top) 1 km and (bottom) 7 km for Hurricane Pali (2016).

The retrieval algorithm consists of two parts: building an a priori database and choosing a profile from the database. The database was created from 10 WRF simulations. Ten tropical cyclones (TCs) in the Atlantic basin with different intensities varying from Category 1 to 4 were chosen arbitrarily (Arthur (2014), Bill (2009), Cristobal (2014), Danielle (2010), Edouard (2014), Gonzalo (2014), Gustav (2008), Igor (2010), Katia (2011), and Omar (2008)) and were simulated in the WRF model with the Advanced Research WRF (ARW) dynamical core for 12 h. WRF-ARW version 3.7 (Skamarock et al., 2008) was used with 1° Global Forecast System (GFS) analysis as an initial condition at the cold start and as a boundary condition throughout the analysis and forecast. The model has two domains of 30 vertical levels with the horizontal resolution of 9 km for outer domain and 3 km for inner domain. Physics that are used in WRF for both the retrieval and the DA experiments are summarized in Table 1. Among 22 microphysical schemes in WRF, the WDM6 scheme was applied following the results from Kim et al. (2013) showing a high correlation with the observed rainfall rates using the WDM6 scheme-based database. Graupel was assigned as the fifth hydrometeor instead of hail for the tropical environment (McCumber et al., 1991). The WDM6 scheme was modified to produce an additional output of vertical profile of LH coming from a phase change between hydrometeors as this is not a general output in WRF. In the modified WDM6 scheme, LH is calculated by dividing a temperature change from any phase change by the appropriate time step. It has a unit of K/s. Since the temperature change used in the calculation is solely from phase changes, temperature change from advection is excluded.

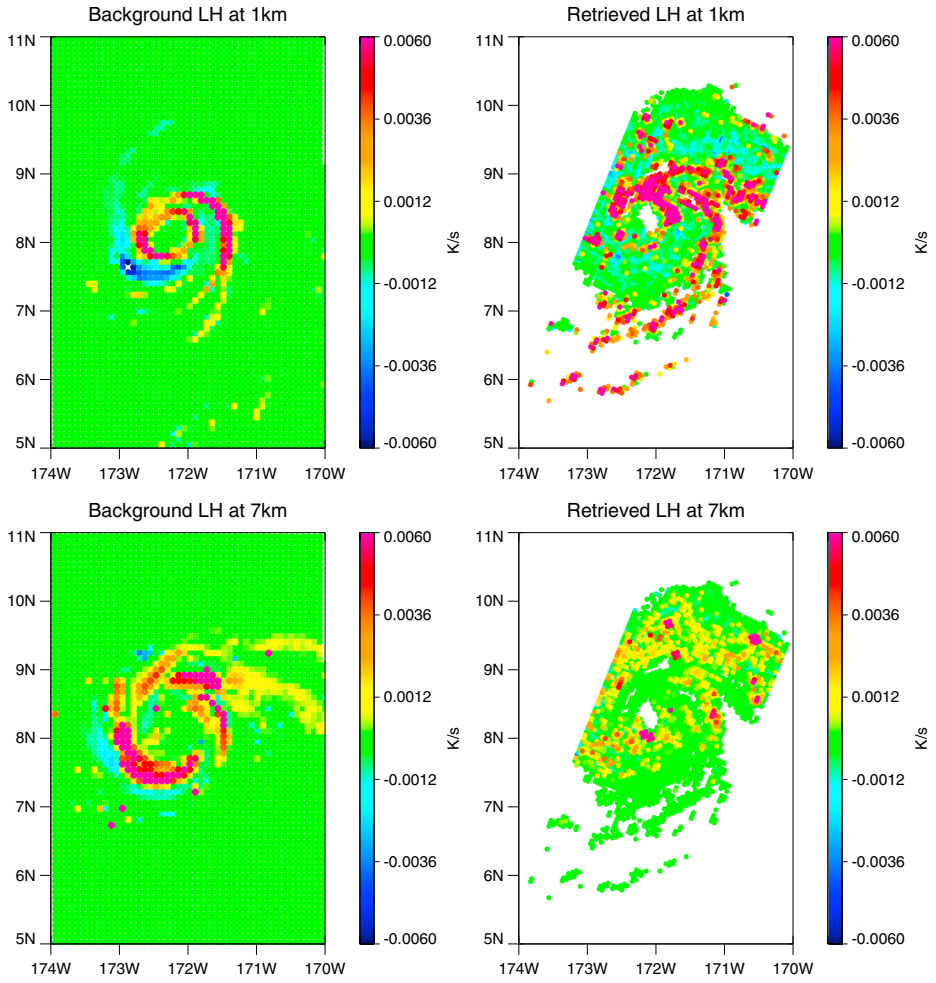

Figure 3. (left) Background and (right) retrieved latent heating horizontal cross section at (top) 1 km and (bottom) 7 km for Hurricane Pali (2016).

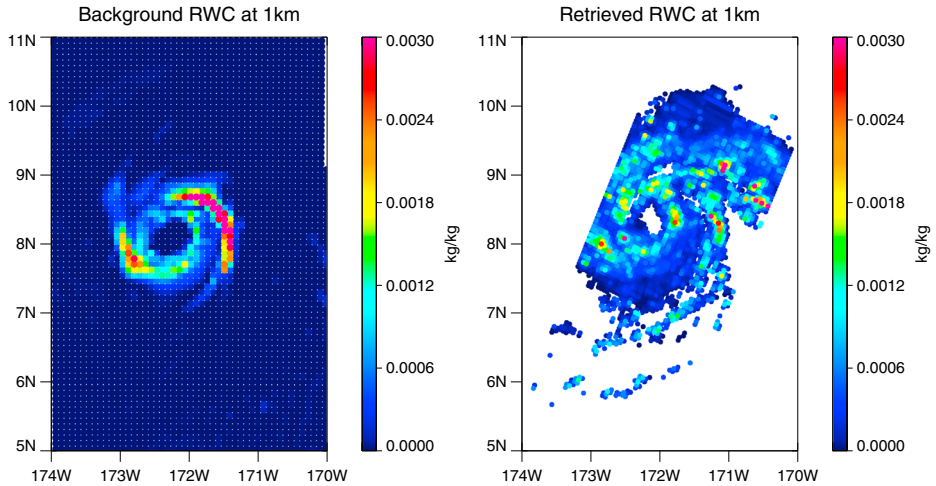

Figure 4. (left) Background and (right) retrieved rainwater content horizontal cross-section at 1 km for Hurricane Pali (2016).

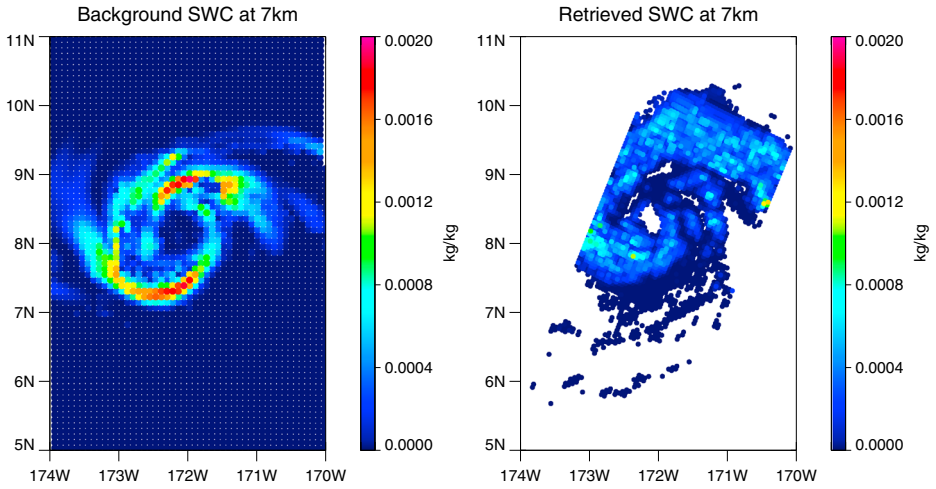

Figure 5. (left) Background and (right) retrieved snow water content horizontal cross section at 7 km for Hurricane Pali (2016).

The calculation of reflectivity requires profiles of temperature, pressure, water vapor, surface wind velocity, hydrometeor water contents, and size distribution as inputs. The Eddington model was used to calculate radiance and reflectivity with inputs provided by the WRF model. The Eddington model has its own emissivity model but it was replaced by the Fast Microwave Ocean Emissivity version 5 model (Bormann et al., 2012) in this study. The exponential size distribution in the Eddington model was also replaced with the WDM6 scheme for each hydrometeor species to be consistent with the WRF outputs. Among calculated vertical profiles of reflectivity, only profiles that contain at least one level of reflectivity exceeding DPR's threshold of 12 dBZ were saved in the database with the associated VV, LH, and HYDRO profiles from the WRF outputs. Those sets of profiles are separated into convective and stratiform (C/S) rainfall system to constrain the database. Because the C/S separation of the operational GPM algorithm is based on both the reflectivity profile and the horizontal texture, this classification adds some additional information. Once the database is created, the observed reflectivity profiles at each pixel are compared with the simulated reflectivity profiles in the database of the corresponding system type. Reflectivity observation of 2ADPR version 4 (V04) is obtained from the Precipitation Processing System (PPS), and reflectivity at 13.6 GHz (Ku-band) was used. The observed reflectivity has 176 vertical layers up to 22 km with

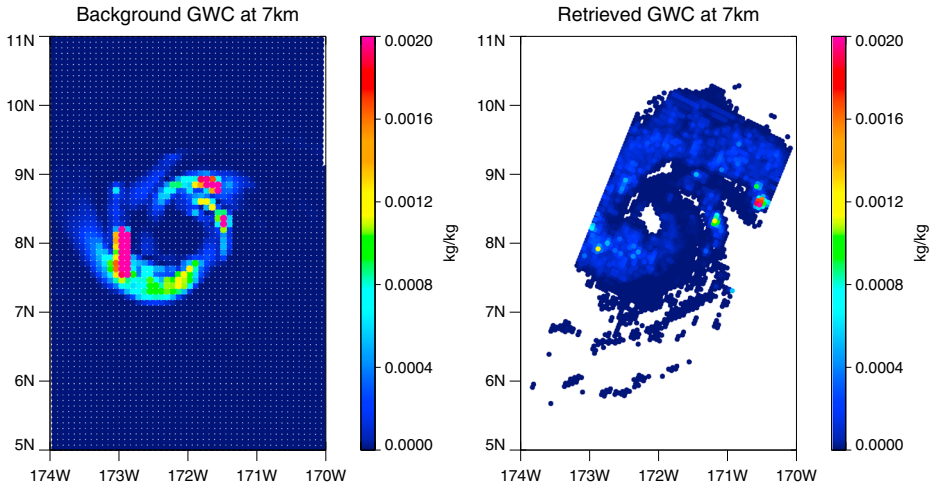

Figure 6. (left) Background and (right) retrieved graupel water content horizontal cross-section at 7 km for Hurricane Pali (2016).

Table 2
Number of Observation and Cost Function Before and After the DA Experiments

		VV	LH	HYDRO
Number of observation		84,434	65,501	137,019
Cost function	Before	3.6523×10^4	2.2923×10^4	5.5692×10^4
	After	2.7523×10^4	1.6334×10^4	4.4252×10^4

0.125 km interval while the modeled reflectivity has 30 layers, and its top layer is located a little over 20 km. Since the observed reflectivity data have finer vertical resolution, they were interpolated to the 30 layers. The squared differences between observed and modeled reflectivity are summed, and profiles with the least squared difference are chosen as "retrieved" fields (VV, LH, and HYDRO) for that grid. In order to smooth these values, they are averaged between six neighboring pixels with a rough Gaussian weight of 0.1 for each neighboring point and 0.4 for the center of the grid.

Generally, in convective systems, both VV and LH are positive throughout the vertical layers due to a strong updraft and consequent condensation. In stratiform regions, on the other hand, the VV below the freezing level is small or even negative, which leads to evaporation and negative LH near the surface, while heating is often maximum at higher levels than in the convective regions. These differences were considered in most LH retrievals as well (Shige et al., 2004; Tao et al., 1993). These LH retrieval algorithms generally assume that the vertically integrated LH due to condensation is proportional to the precipitation rate. This might be true in a broad, or long time average sense, but precipitation at a specific time step actually comes from the condensation prior to that time step. In addition, using rainfall rate to estimate LH might not be the best approach in tropical cyclone cases where convective and stratiform regions are mixed in their rainbands. In the mature stage of the tropical cyclone, stratiform regions where subsidence or weak updraft dominates can also have significant amounts of surface rain rate. For these reasons, some studies use VV as an indicator of the types of systems. Atlas et al. (2000) used VV of 1 m/s for a partitioning of the tropical oceanic systems. Sui et al. (2007) did not use VV for the partitioning, but showed in their paper that convective and stratiform structures have clearly different features of average VV profile. Therefore, VV at 1 km is used for the C/S partitioning in this study. If the VV is greater than 0.5 m/s, it is classified as convective and the remainder is classified as stratiform.

3. Experimental Setup

3.1. Case Description

Two hurricanes that developed in the Pacific basin were chosen as a proof of concept study. They are Hurricane Pali (2016) and Jimena (2015), and both hurricanes were captured by the GPM satellite.

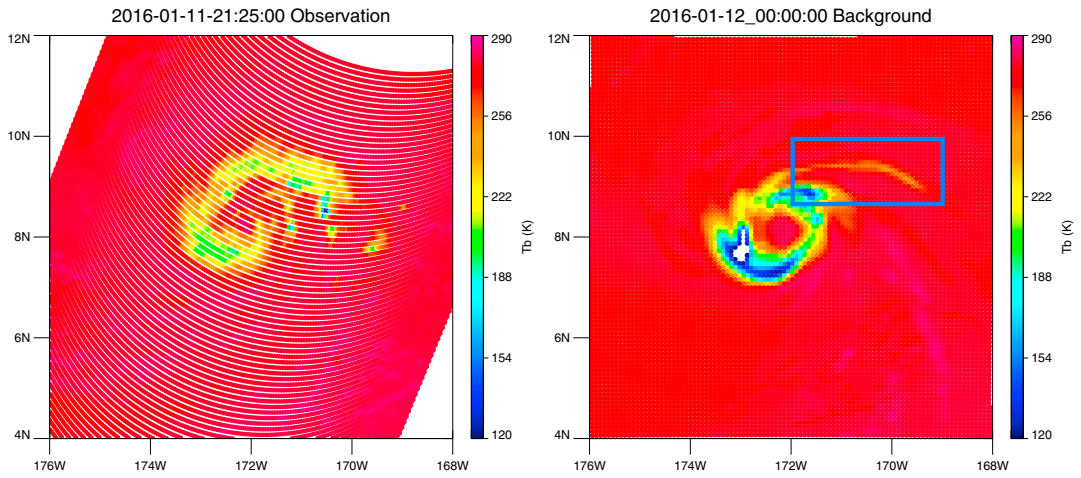

Figure 7. T_b map of observation and the background at 89GHz V for Hurricane Pali (2016).

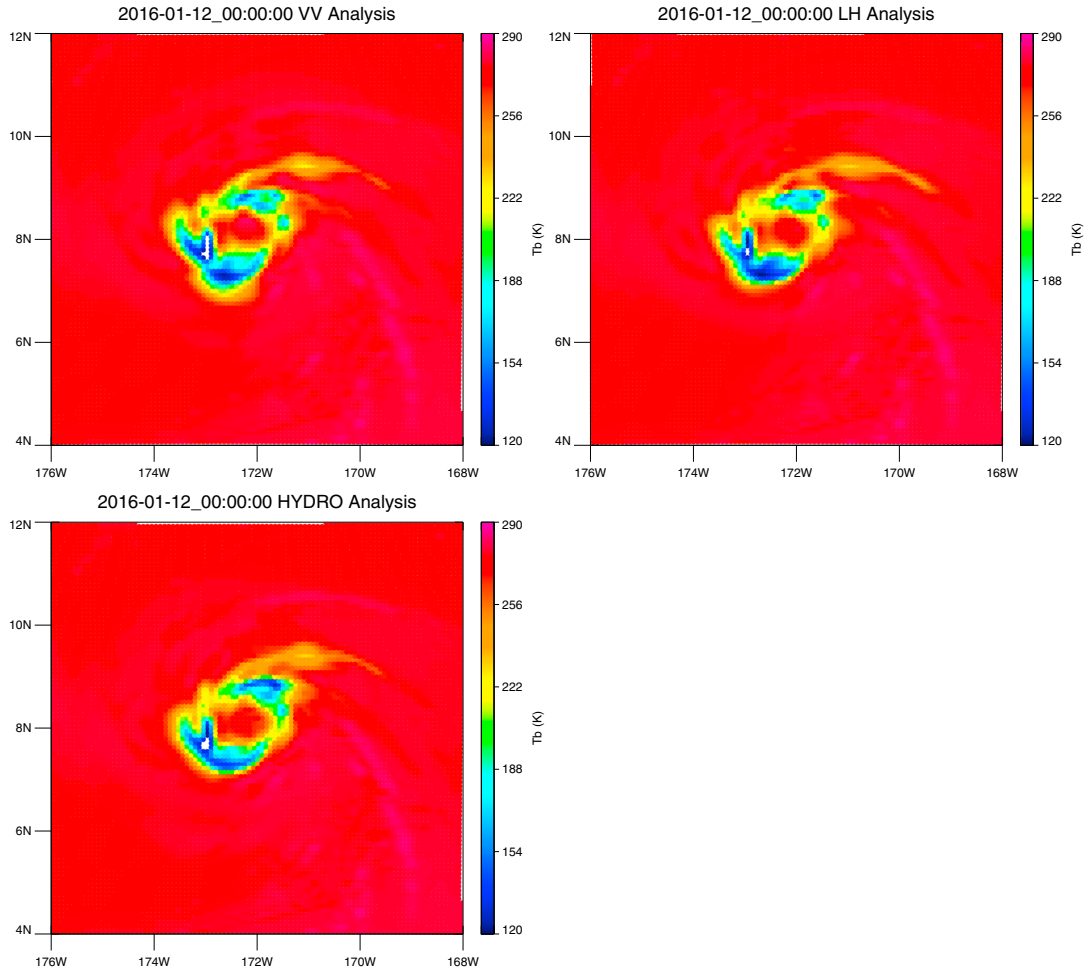

Figure 8. T_b map of VV, LH, and HYDRO at 89 GHz V for Hurricane Pali (2016).

Hurricane Pali (2016) developed over the central Pacific basin on 7 January 2016. It strengthened to a Category 1 hurricane on 11 January, becoming the earliest hurricane on the record (Climate Council of Australia, 2017) and was upgraded to Category 2 on 12 January. It weakened to a tropical storm as it moved southward and dissipated on 15 January. Hurricane Jimena (2015) was stronger and lived longer than Pali (2016). It developed in the eastern Pacific basin on 26 August 2015 and rapidly deepened to Category 1 hurricane in 48 h. It strengthened to a Category 4 hurricane on 29 August reaching its peak wind speed of 135 kt, just below Category 5 status. Jimena (2015) stayed as a Category 4 hurricane for several days, undergoing an eyewall replacement cycle. After that, it slowly weakened as it moved further toward the west and dissipated on 10 September.

3.2. Assimilation Setup

The Maximum Likelihood Ensemble Filter (MLEF) method is used as the DA system. The MLEF is an ensemble-based DA method that also includes components of variational data assimilation, such as the minimization of the cost function. An ensemble method is suitable for hurricane predictions because it includes flow dependency of the forecast error covariance. Flow dependency allows the MLEF to include cross correlations between control variable uncertainties, and therefore produce a dynamically-constrained adjustment. Details of the MLEF can be found in Zupanski (2005) and Zupanski et al. (2008). The MLEF was compiled with the same WRF model described in section 2 and run with 32 ensemble members. The WRF model used in DA has different horizontal resolution from the WRF model used in retrieval. Such experimental design corresponds to the so-called "nonidentical twins" setup. Unlike identical twins, the nonidentical twins imply that

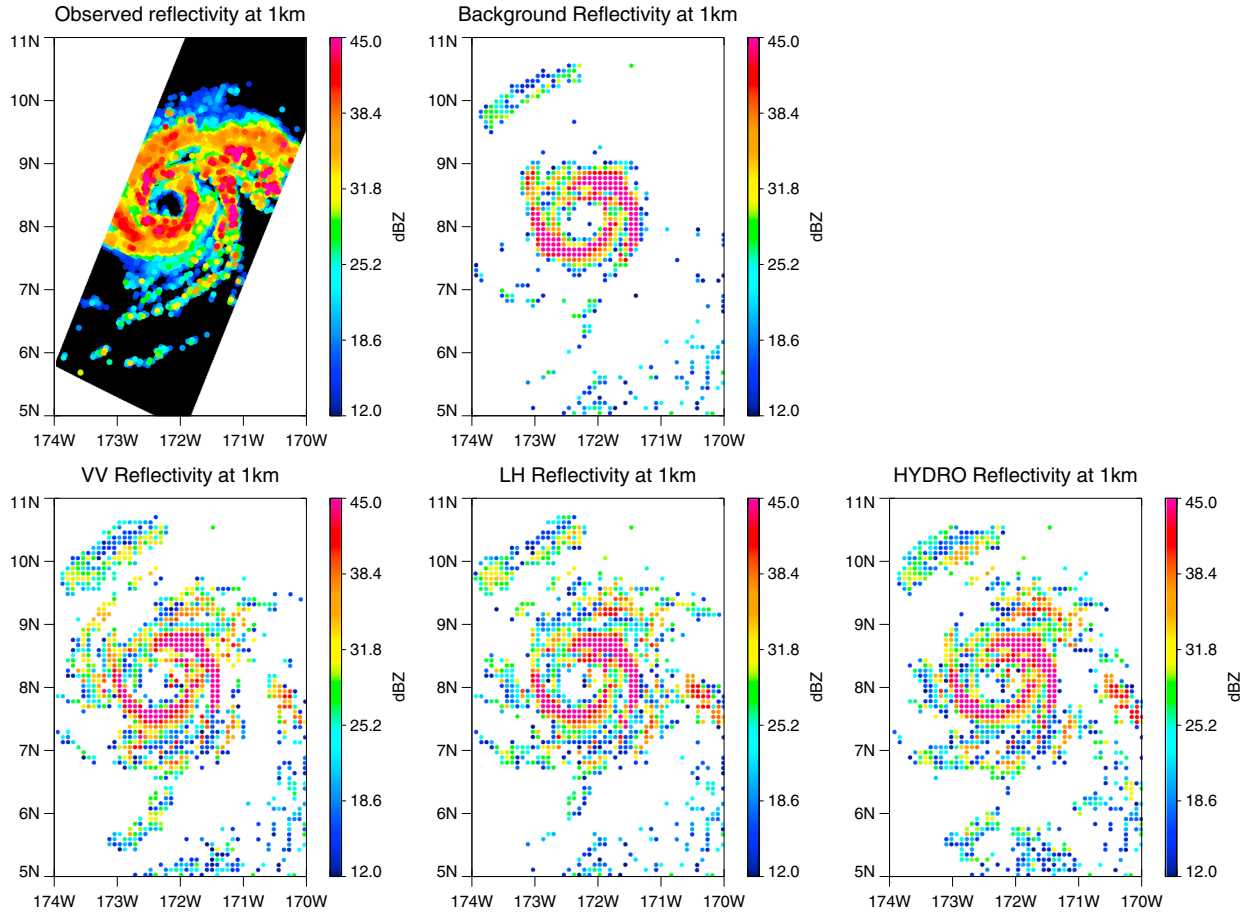

Figure 9. Horizontal cross section of reflectivity at 1 km for observation, background, VV, LH, and HYDRO.

the forecast model used in assimilation is not perfect, and thus, the experiments are more realistic. The WRF model in the DA simulations has two domains with 30 vertical levels, as in the retrieval, but each domain has fewer grid points with a coarser resolution (27 km for the outer domain and 9 km for the inner domain). Each simulation assimilates one of the three variables, but the control variables for all of the simulations are kept the same. Control variables include the WRF model variables (perturbation potential temperature, perturbation geopotential, horizontal velocities, and perturbation dry air mass in column) and variables that will be assimilated (VV, LH, and HYDRO). The observation operator is a spatial interpolation from model grid to observation location for all three variables.

Quality control (QC) of observational data for each parameter is slightly different. The common QC for all parameters is to reject observation data that are too far from the model. Observation data passes the QC check if the following condition is satisfied.

$$\frac{|y - \boldsymbol{H}(\mathrm{x})|}{\sqrt{\mathbf{R}}} < 3 \quad \text{where}$$

y : observation vector
x : state vector
$\boldsymbol{H}$: observation operator
$\mathbf{R}$: observation error covariance matrix

Observation errors that comprise diagonal elements of R are empirically determined and set to constant values of 0.3 m/s, 0.001 K/s, and 0.0001 kg/kg, for each VV, LH, and HYDRO, respectively. More details are mentioned in section 4.3. As an additional QC for LH and HYDRO, observations are assimilated if the absolute values of both observed and modeled data are bigger than the threshold of 10^{-6} (K/s for LH and kg/kg for HYDRO). This was done to make the probability distribution of the innovation vector ($y - \boldsymbol{H}(\mathbf{x})$) Gaussian, as is assumed in MLEF. Without this process, the distribution becomes more like a leptokurtic curve that

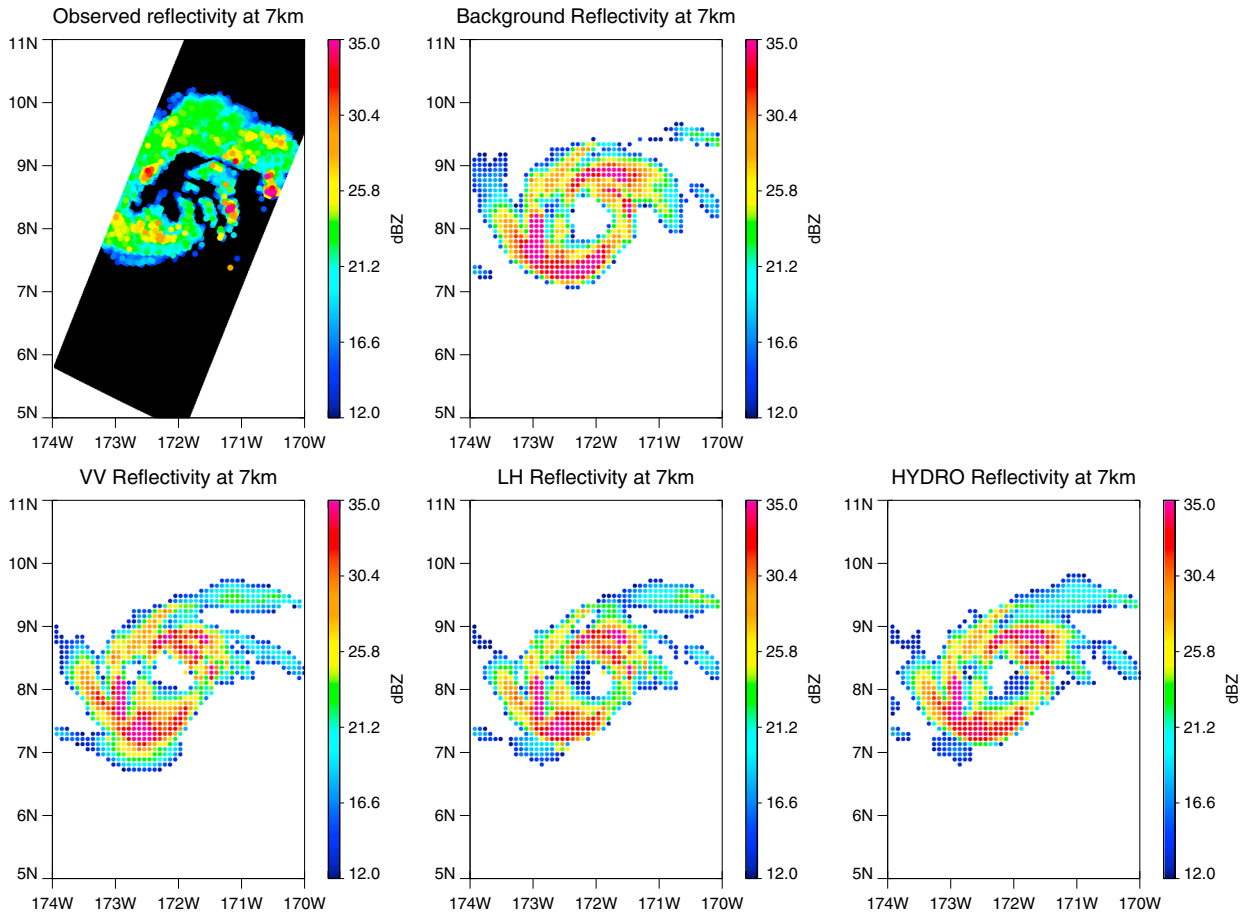

Figure 10. Horizontal cross section of reflectivity at 7 km for observation, background, VV, LH, and HYDRO.

peaks around 0 because the system incorporates unnecessary data that just exist to increase the frequency around 0 such as rainwater content above the freezing level or ice hydrometeor content below the freezing level. VV does not require this procedure because it has nonzero values most of the time. However, since it is given at layer boundaries instead of averaged over the layer, and MLEF uses a system that assimilates observation data averaged over layers where most control variables reside, it requires an additional treatment for the vertical staggering. Thus, VV either has to be interpolated into layers or a way to process VV at the layer interfaces must be implemented. In order to avoid the vertical interpolation that might bring in more noise, the top level of VV is discarded and the remaining observation values are assumed to be the values at the upper layers.

With this assimilation setup, three different experiments were conducted to assimilate each variable that was retrieved when the GPM satellite passed over each hurricane: VV, LH, and HYDRO. Background data and control variables are identical for the three experiments to make a simple comparison between different assimilated retrievals. The GPM satellite passed over Hurricane Pali (2016) at 2125 UTC 11 January 2016 while it captured Hurricane Jimena (2015) at 1011 UTC 1 September 2015. In order to make these data lie within the 6 h assimilation window, analysis time was set as 0000 UTC 12 January 2016 and 1200 UTC 1 September 2015 for Hurricane Pali (2016) and Jimena (2015), respectively.

4. Results

4.1. Results for Hurricane Pali (2016)

With clouds seen in Hurricane Pali (2016), the retrieval algorithm produced 92,940 observation data for LH and HYDRO and 96,038 data for VV (92940 points after passing the QC that discards data at the top level). These data cover regions from the convective core of the hurricane to rainbands around the core. Figure 1

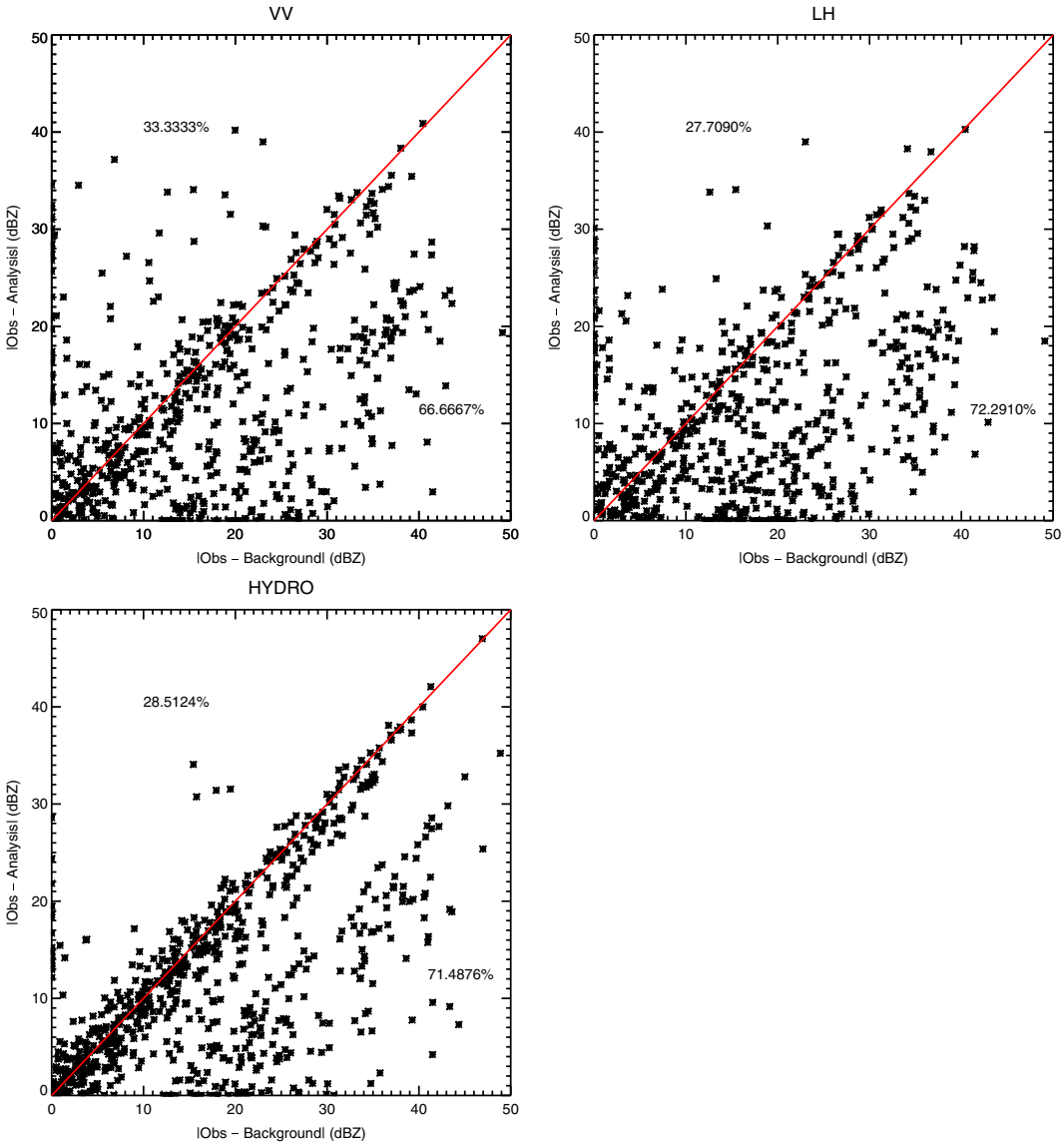

Figure 11. Scatterplot of absolute difference between observation and analysis against absolute difference between observation and background for VV, LH, and HYDRO excluding points that did not change significantly.

shows the reflectivity of the best matches from the a priori database and the observed reflectivity from DPR at two different vertical levels. The lower level is at 1 km, and it describes the liquid precipitation in the scene while the higher level, at 7 km, is above the freezing level and represents a mixed-phase scene composed of ice and supercooled liquid hydrometeors. While a perfect a priori database would fully match the observed reflectivity structure, there are some differences. The retrieved reflectivity captures the raining portion of the profile (high reflectivity) well enough, but reflectivity above the freezing level is not as representative as in the lower level. The reflectivity from the best match is overestimated at 7 km. This might be due to an overestimation of ice hydrometeors from the database, a well-known problem in the forecast models (Gallus & Pfeifer, 2008; Han et al., 2013).

Horizontal maps of the retrieved fields of the three variables are compared with the background model data next. In Figure 2, VV from the background at 1 km shows clear updrafts and downdrafts around the rain-bands. As in the background, the retrieved VV shows bands of updrafts and downdraft. The retrieved VV may be more reasonable than the background because the updraft region in the retrieved field matches the region with high observed reflectivity especially at 7 km.

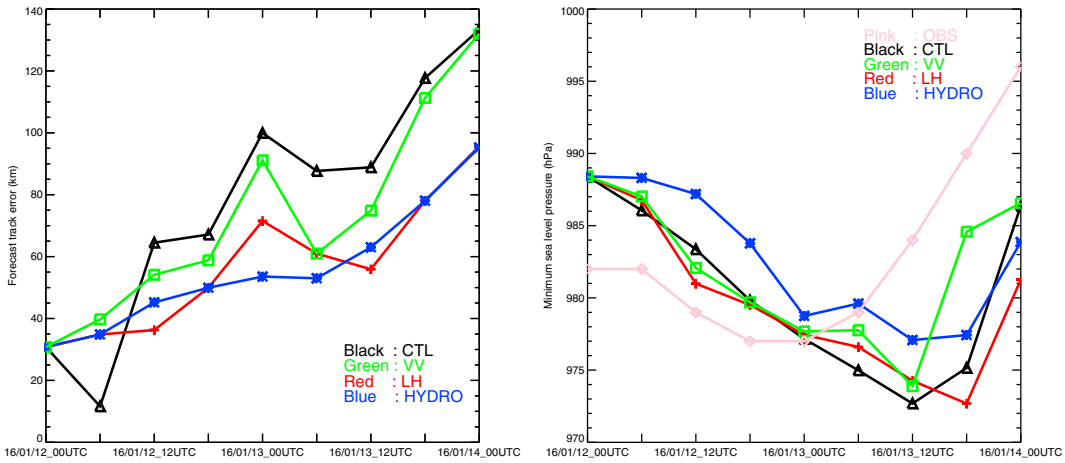

Figure 12. Hurricane Pali (2016) forecast track error (left) and MSLP (right) for CTL, VV, LH, and HYDRO runs.

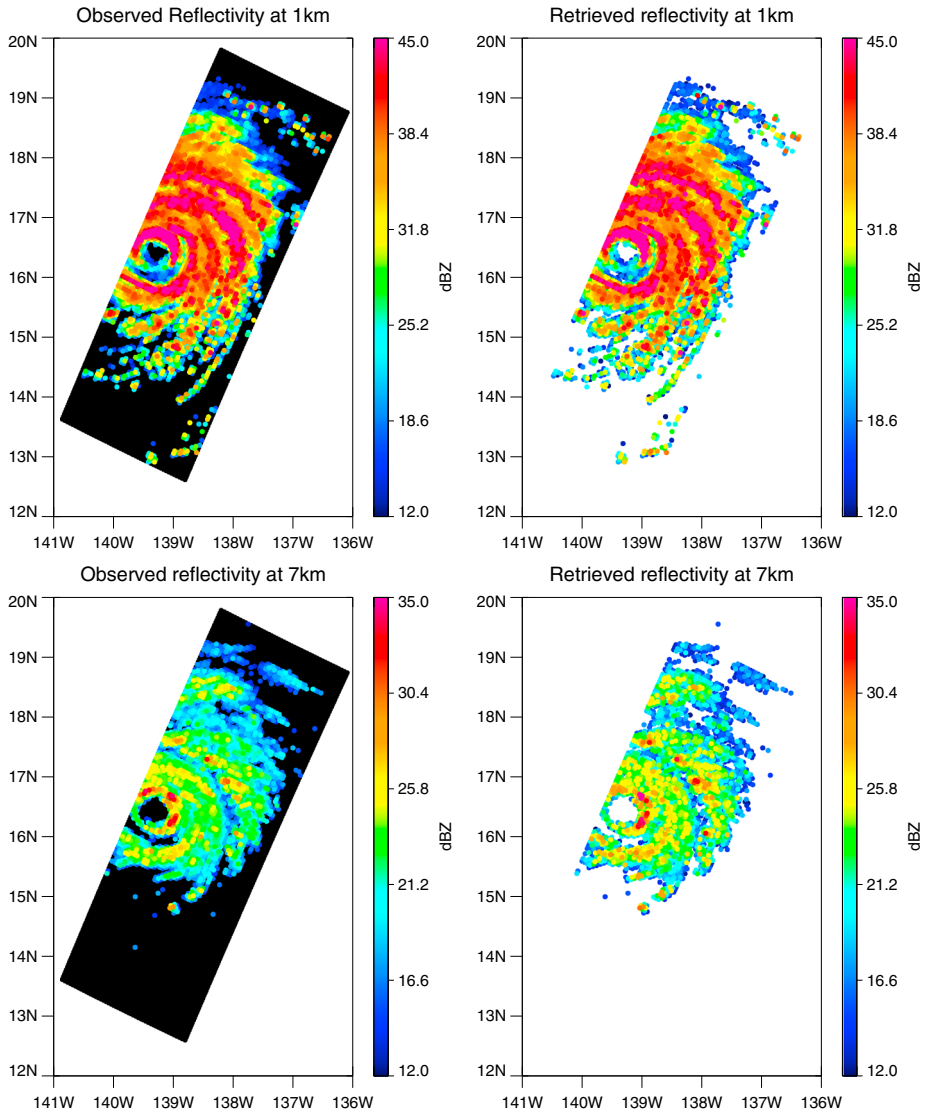

Figure 13. (left) Observed and (right) retrieved reflectivity horizontal cross section at (top) 1 km and (bottom) 7 km for Hurricane Jimena (2015).

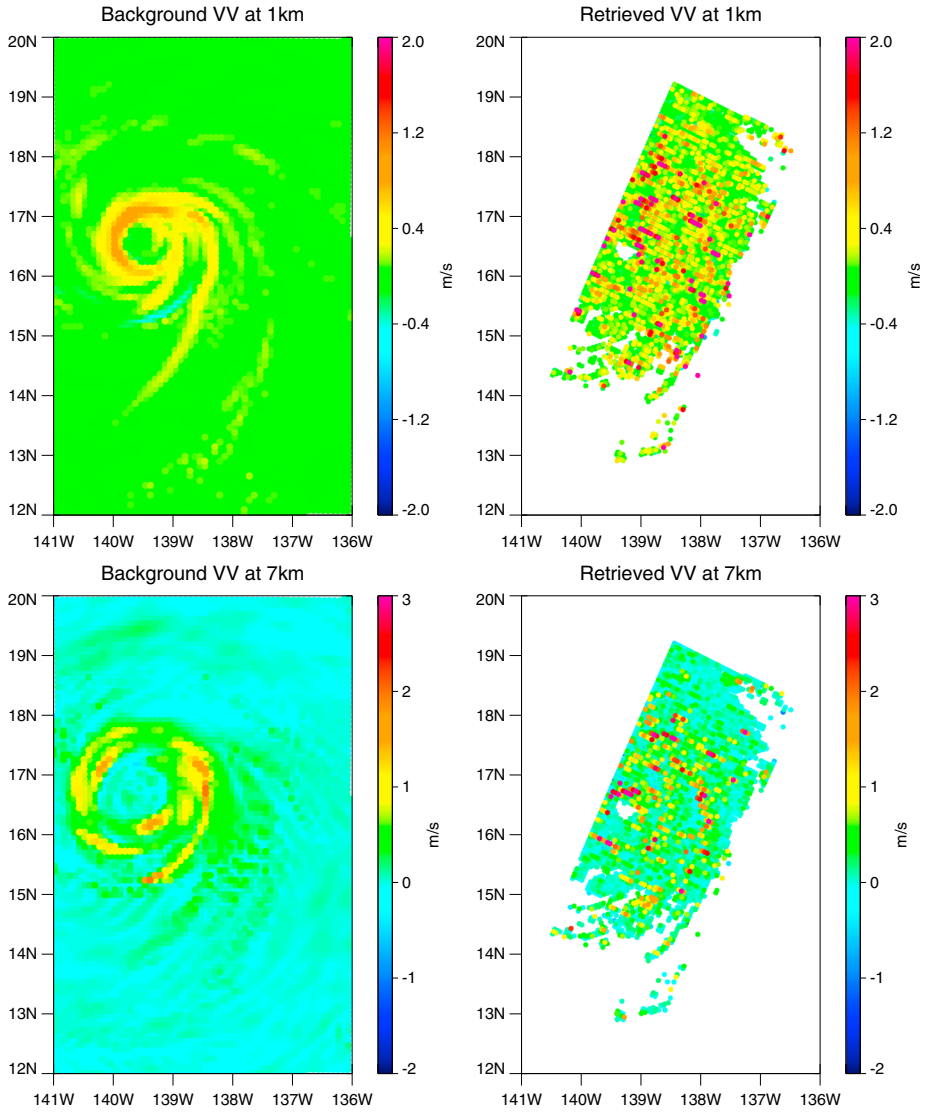

Figure 14. (left) Background and (right) retrieved vertical velocity horizontal cross section at (top) 1 km and (bottom) 7 km for Hurricane Jimena (2015).

In Figure 3, the background and retrieved fields show similar pattern of LH at both levels although the heating is substantially larger at 7 km in the background field. They both show convective (positive LH at the cloud base that slowly decreases with height in the rainbands) and stratiform (negative LH at the cloud base due to evaporation and positive at upper level) features between rainbands. At 1 km, positive and negative LH appears between rainbands while it is mostly positive at 7 km. LH agrees well with the VV map in both background and retrieved fields. Updraft regions correspond to the region with positive LH, implying condensation or freezing, and regions with a downdraft show negative LH due to evaporation or melting.

Hydrometeors follow the reflectivity pattern most closely as they are directly related to the reflectivity. Precipitating hydrometeors were only examined at the level where they exist (rain at 1 km and snow and graupel at 7 km). Rain water content at 1 km is somewhat more dispersed than the background field that shows very narrow bands of rainwater contents, as shown in Figure 4. At 7 km, snow and graupel (Figures 5 and 6) also show a more diffuse pattern that is typical of TCs. However, in the retrieved field, high concentrations of snow and graupel are not shown at 7 km even in areas of strong convection. Its low concentrations are consistent with low reflectivity in Figure 1 and can be attributed to Pali (2016) being a weak Category 2 hurricane. Overall, the retrieved data looks reasonable to represent the real TC system.

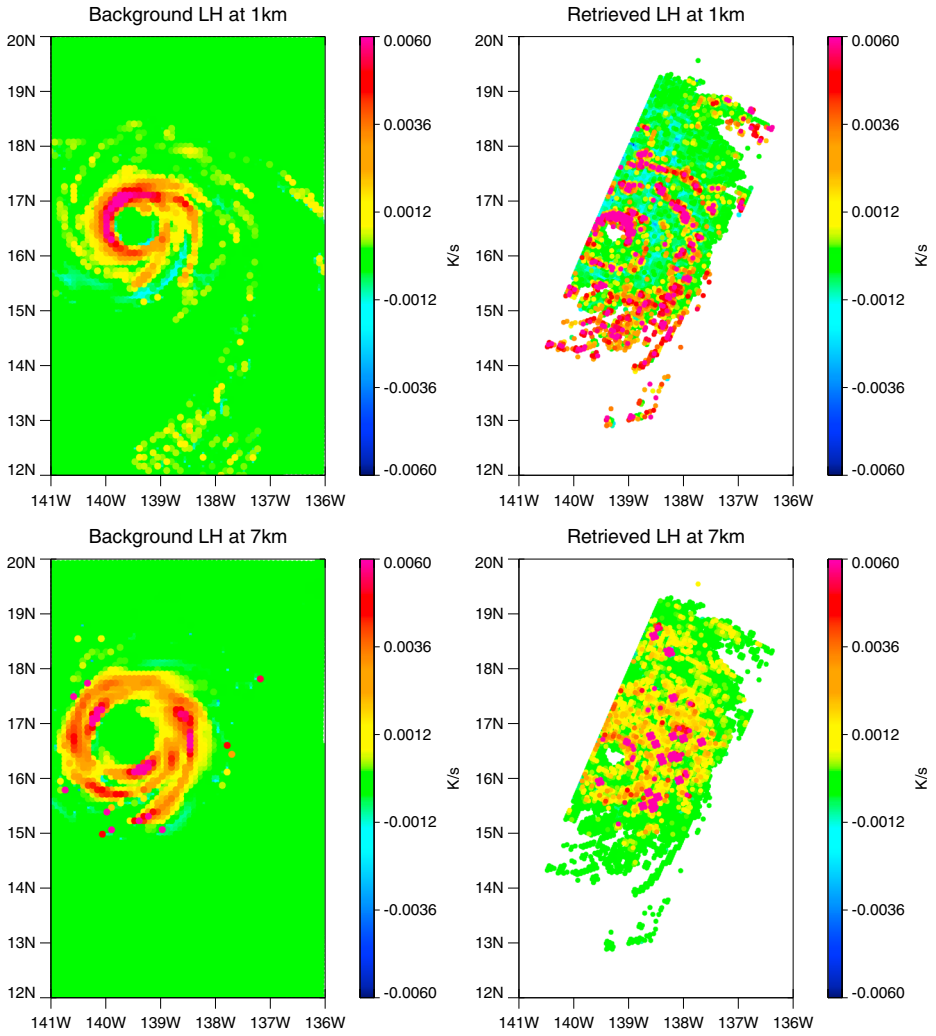

Figure 15. (left) Background and (right) retrieved latent heating horizontal cross section at (top) 1 km and (bottom) 7 km for Hurricane Jimena (2015).

The number of observations that passed QC for the inner domain with 9 km resolution is shown in Table 2. Individual hydrometeor species have fewer observations that passed QC because they only exist within certain levels, but the total amount of entries is highest for HYDRO when cloud water, rain, ice, snow, and graupel are counted.

The total cost function that includes observation and background terms was calculated before and after the DA simulation in order to examine the improvements. A lower cost function means that the difference between observed and modeled variables decreased, thereby improving the quality of the analysis. Cost functions decreased by 25%, 29%, and 21% for VV, LH, and HYDRO, respectively. All of the experiments show decrease in the cost functions meaning that the DA worked and the analysis more closely resembles the observations after assimilation.

Analysis vectors produced after the DA experiments were examined with independent observations for an objective validation. T_b from GPM Microwave Imager (GMI) can be used for independent verification purposes. Level 1C GMI data V04 were obtained from the PPS. For a comparison between the observed T_b and the T_b calculated based on the analysis and background, T_b at 89 GHz (vertical polarization) was used because this channel is sensitive to hydrometeors, especially in the ice phase. In Figure 7, the model background correctly created the convective core of the hurricane in the observed location, but it overestimated ice hydrometeors around the rainbands, and did not create the rainband in the blue box. Overestimation of

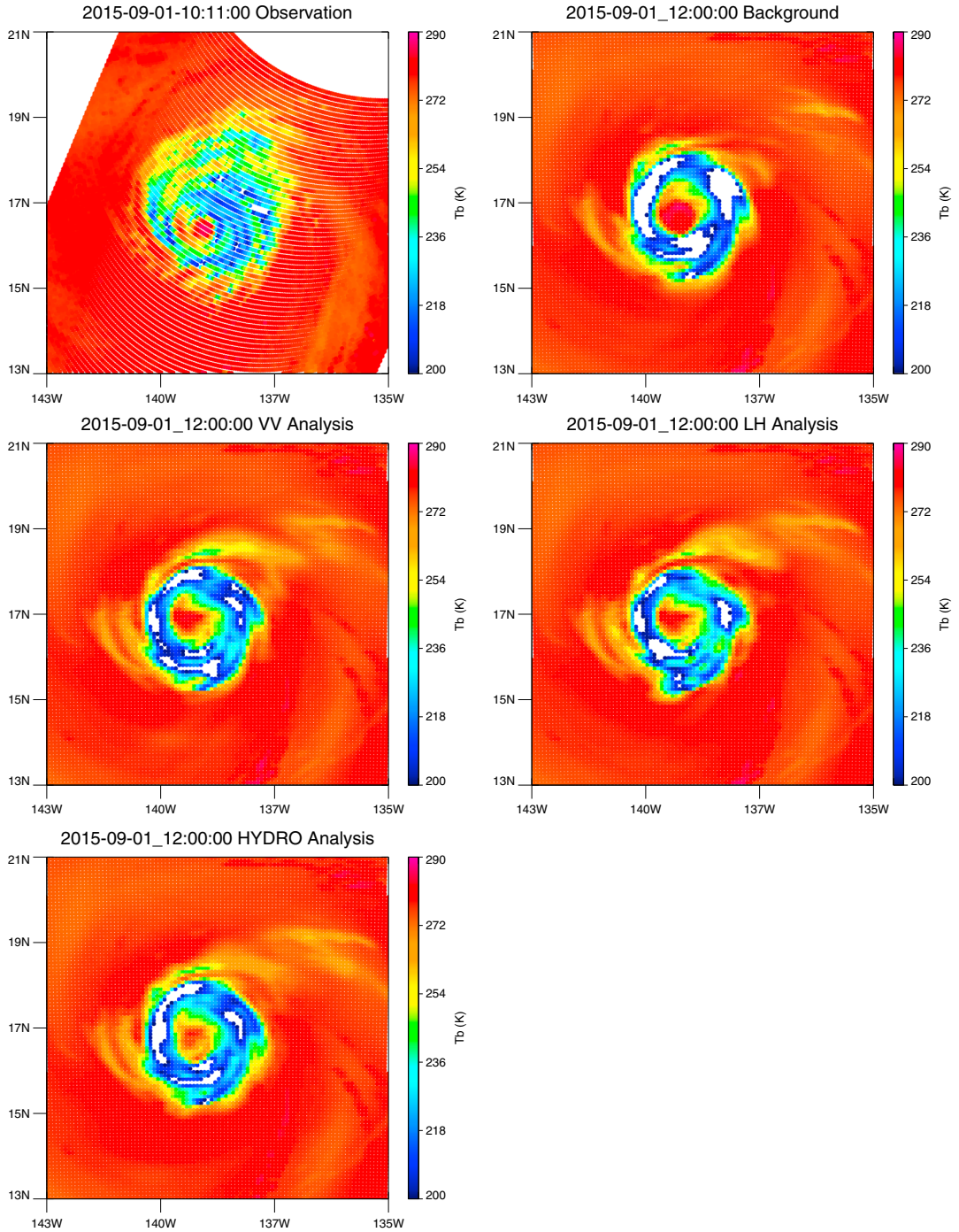

Figure 16. T_b map of observation, background, VV, LH, and HYDRO runs at 89GHz for Hurricane Jimena (2015).

ice hydrometeors is evidenced by lower T_b caused by too much scattering of radiation away from the viewing direction. Figure 8 is the same T_b map but with VV, LH, and HYDRO run. VV run seemed to create the upper part of the rainband but still significantly overestimates the amount of ice scattering as in the background. In addition, it moved the lower part of the rainband southward, which should have been moved northward. By contrast, the LH run reduced the amount of ice scattering considerably and created the upper rainband. It even tried to reshape the lower part of the rainband to better fit observations. HYDRO run showed a similar pattern as LH run but with less scattering at the lower rainband and higher scattering at the upper rainband.

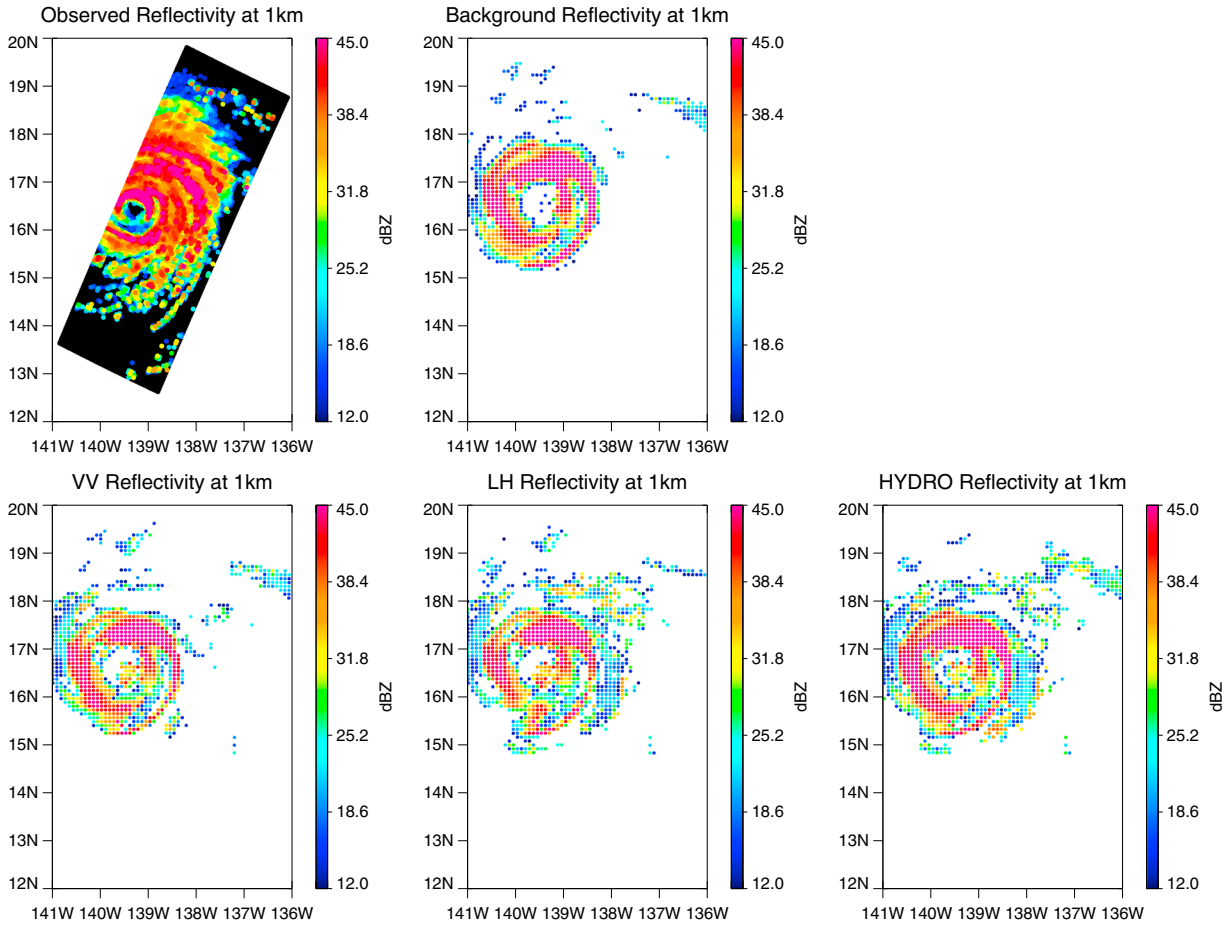

Figure 17. Horizontal cross section of reflectivity at 1 km for observation, background, VV, LH, and HYDRO.

In addition to the T_b, DPR reflectivity can also be used for validation data although it was used in the retrieval of the assimilated parameters. It is nonetheless useful in the sense that it can be evaluated at different levels. Figures 9 and 10 show reflectivity before and after the DA experiments at 1 km and 7 km, respectively. Background reflectivity at 1 km appears discontinuous at the edge of the rainbands. All three experiments improved the simulation by creating trailing rainbands at 1 km. At 7 km, all three experiments showed similar patterns between the three experiments. They produced ice hydrometeors in the north east part of the rainband but, at the same time, they created unnecessary ice at the south of the rainband around 7°N. One thing to note here is that the results for LH and HYDRO look very similar both at 1 km and 7 km.

Figure 11 provides a quantitative assessment of the improved analysis for the VV, LH, and HYDRO assimilation experiments, respectively. The horizontal axis in each plot displays the absolute difference between the observations and the background reflectivity while the vertical axis is the absolute difference between the observations and the analysis. Points to the right of the one-to-one line therefore show an improved analysis field. A significant amount of points were on the one-to-one line (76.9%, 57.0%, and 56.8% for VV, LH, and HYDRO, respectively), and they were removed from the figure for convenience. Those points might appear to be unaffected by the DA procedure, but it is more likely that the change is very subtle and not detectable on the plot. All three experiments showed some improvements. In the VV experiment, 15.4% of the points improved in the analysis while 7.7% became worse and the remaining 76.9% were unchanged. Of those that changed, 66.7% showed improvement and 33.3% retrograded. In the LH experiment, 31.0% of the total points improved. Excluding the points on the one-to-one line, it shows 72.3% improvement. HYDRO experiment also shows 71.5% of improvement without the unchanged points. The number of points that passed QC was larger in the HYDRO run than with LH, making HYDRO the most influential variable. The reason

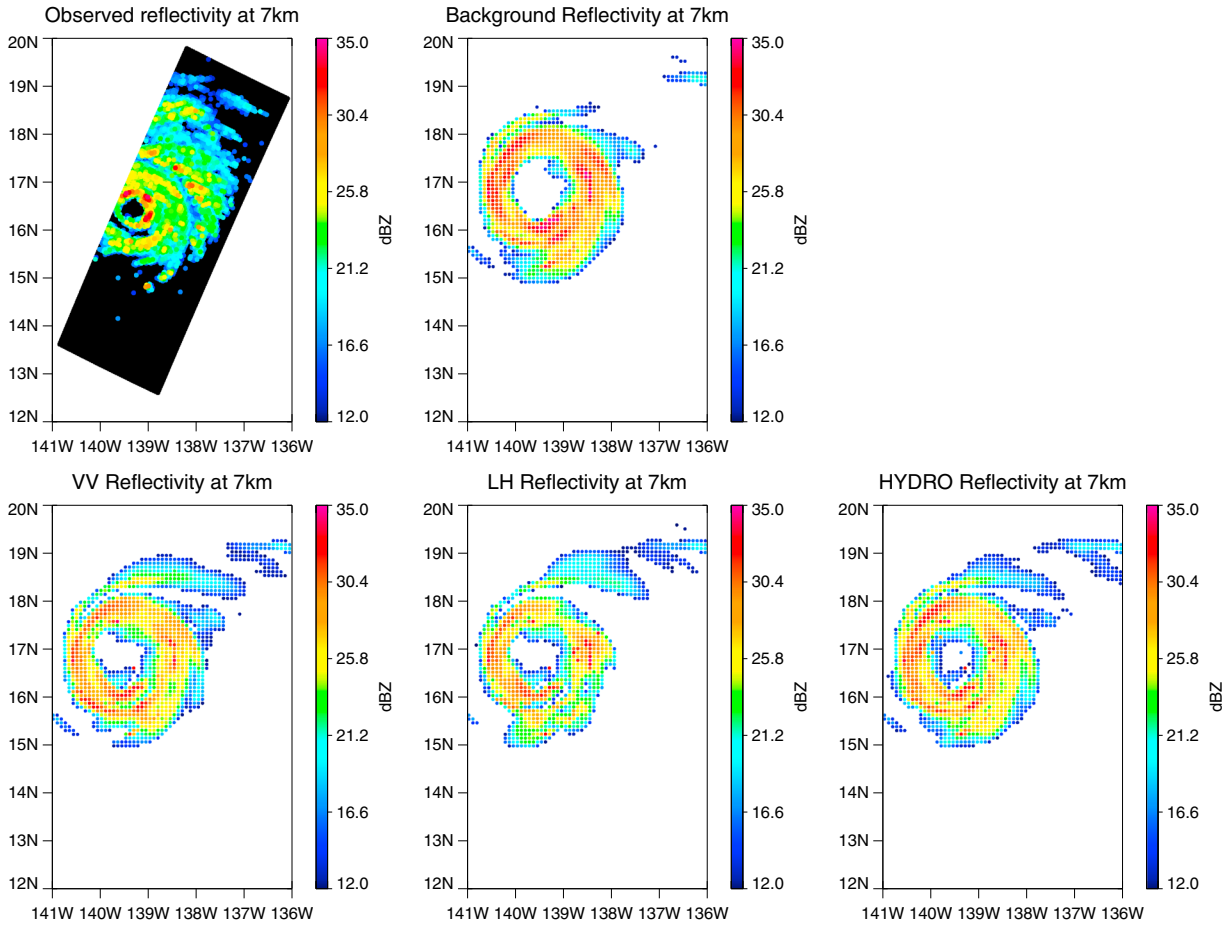

Figure 18. Horizontal cross section of reflectivity at 7 km for observation, background, VV, LH, and HYDRO.

that HYDRO had the most positive impact on reducing the discrepancy in reflectivity might be because hydrometeor water contents are directly related to the reflectivity calculation as an input in the RTM. Although HYDRO had the most positive impacts, it is hard to conclude from this results that it was the most effective variable because HYDRO experiments assimilated more data.

In addition to evaluating the analysis result, one more experiment was conducted to evaluate if the assimilations led to improvements in the track and intensity forecast. The intensity can be represented by a minimum sea level pressure (MSLP), and the storm track was determined by the location of MSLP. Best track data were obtained from the Automated Tropical Cyclone Forecast (ATCF) (Sampson & Schrader, 2000) system database. It contains locations of the best track and the MSLP every 6 h, and thus, forecast results are plotted with 6 h interval. The WRF model initialized with the analysis from each DA experiment was run for 48 h, and its track error and intensity forecast are plotted in Figure 12. All experiments, including the control (CTL) run, started from the same location because the DA experiments did not change the location of the convective core as shown in previous figures. The CTL run was the closest to the best track data after 6 h but began to deviate after that. Assimilating VV did not improve much on the track forecast but was better at forecasting the intensity overall. LH and HYDRO runs had similar tracks (not shown) and the least error throughout the forecast.

4.2. Results for Hurricane Jimena (2015)

A set of identical experiments were conducted for Hurricane Jimena (2015) starting with the creation of a retrieved data set. Jimena (2015) was a bigger and stronger hurricane than Pali (2016) as is shown in Figure 13. This can be supported by a map of the VV in Figure 14 showing positive values in all the identifiable rainbands in the retrieved profiles and strong condensation occurring around the north side of the

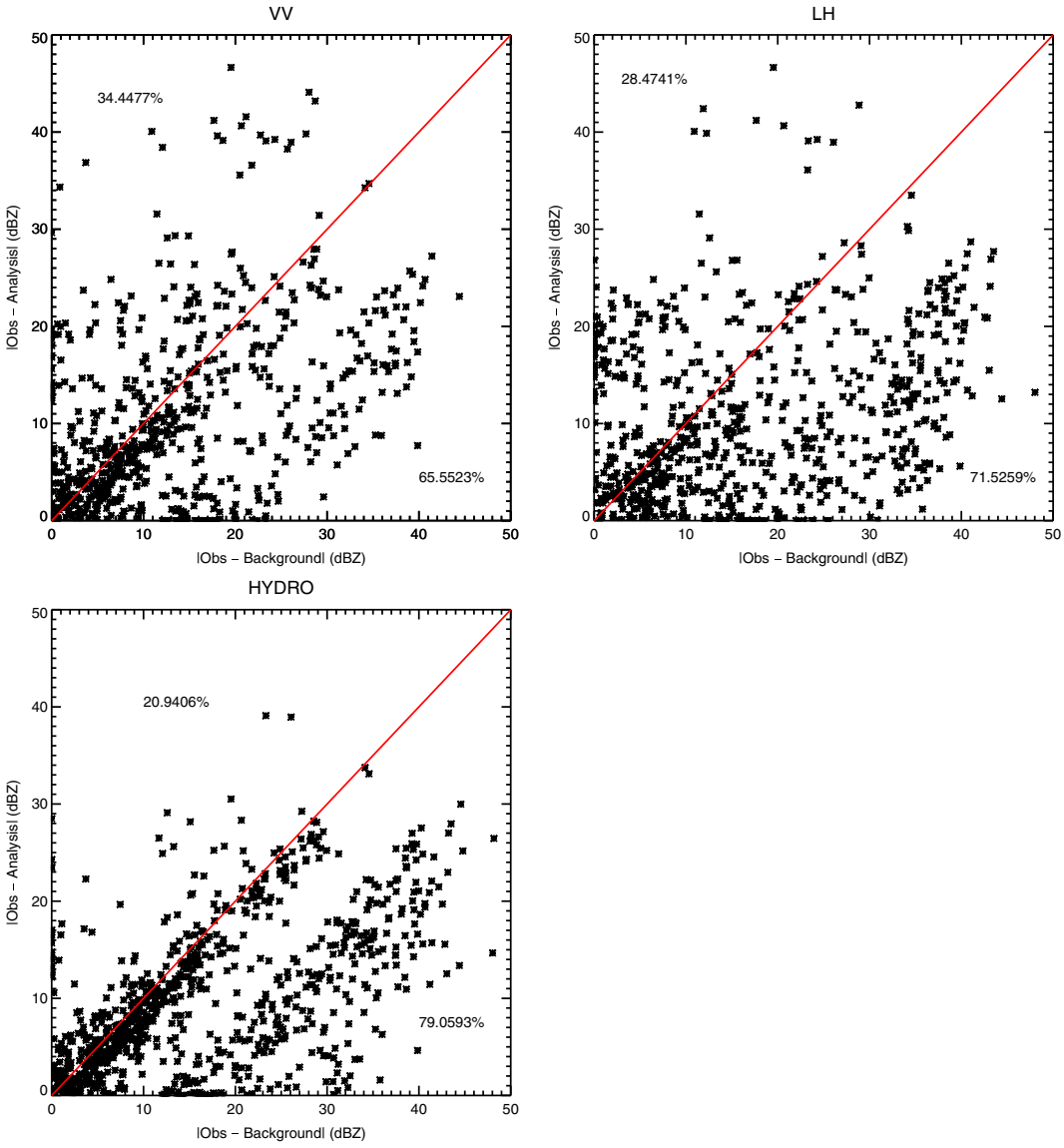

Figure 19. Scatterplot of absolute difference between observation and analysis against absolute difference between observation and background for VV, LH, and HYDRO excluding points that did not change significantly.

convective core in Figure 15. Although it is not straight forward to separate convective and stratiform regions in the VV map because most of the regions show positive VV, these regions are evident in the LH map. HYDRO maps are not shown since they are very similar to the reflectivity map. All of the three retrieved fields seem to capture the hurricane reasonably well. The background model field, on the other hand, had a larger convective core and narrower rainbands. Therefore, a key point in Jimena's case would be whether DA is able to reduce the core size and create a broader rainband structures.

By looking at the T_b at 89GHz in Figure 16, we can see that all of the experiments tried to reduce the convective core size and the ice scattering in the rainband. For evaluating the vertical structure of the TC system after the DA experiments, horizontal cross sections of reflectivity are shown in Figures 17 (at 1 km) and 18 (at 7 km). The background simulation at 1 km is not well developed in the northeastern part of the system. At 7 km, it has generally higher reflectivity than the observations in the rainbands but completely misses the northern part of the rainbands (18.5°N). All three experiments had a positive impact at higher levels by lowering the ice contents, and thus the reflectivity, but creating ice hydrometeors in the northern part of the system. However, VV did not have much impact at the lower levels while the other two experiments expanded the

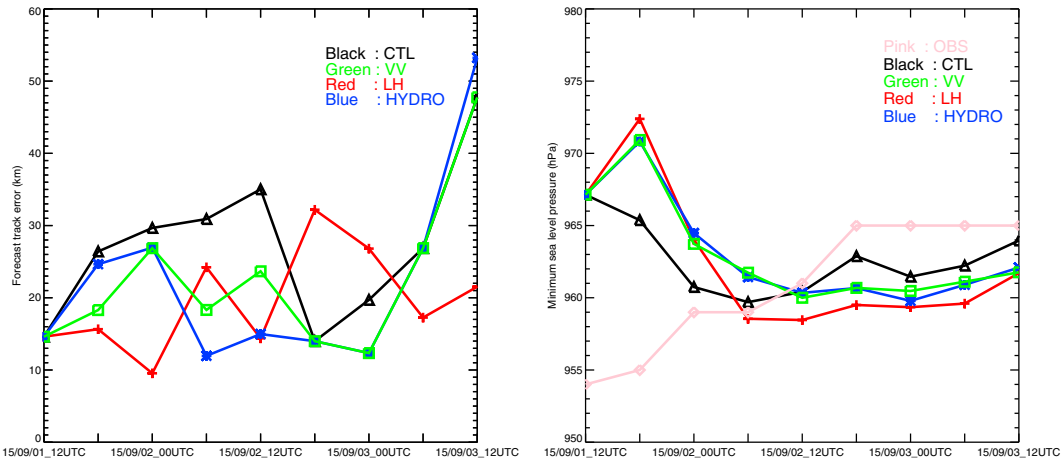

Figure 20. Hurricane Jimena (2015) forecasts (left) track error and (right) MSLP for CTL, VV, LH, and HYDRO runs.

rainbands. The LH and HYDRO assimilation experiments showed similar patterns regarding reflectivity just like in the Pali experiments.

The reflectivity data were again plotted on a scatterplot to evaluate the improvements quantitatively. The percentage of data that contributed to lower difference between observed and analyzed reflectivity, excluding points on the one-to-one line, was 65.6%, 71.5%, and 79.1% of the pixels that showed changes for VV, LH, and HYDRO (Figure 19), respectively. Numerical results show that the HYDRO experiment had the most improvement.

Track and intensity forecasts of the analyses are compared with the best track data from the ATCF database, and it is shown in Figure 20. Similar to the Pali results, LH and HYDRO runs better forecast the track at different time steps. However, in this case, LH run seemed to predict the track a little bit better than HYDRO run throughout the 48 h forecast. Regarding the intensity forecasts, none of the assimilation runs seemed to have improvements compared to the CTL run, but still VV run did better among the three experiments. These results are intuitive because VV is directly related to an updraft, and therefore to the intensity of the system. Some studies showed improvement in the hurricane intensity by assimilating data related to vertical velocity. Li et al. (2012) assimilated radial velocity and showed improvements in the hurricane intensity but not much in the track forecast. On the other hand, some studies show improvements in the track forecast but less in the intensity. Anisetty et al. (2014) assimilated the Global Positioning System (GPS) radio occultation data and showed such results. Since radio occultation data give vertical profiles of temperature, it is more related to LH, and their results agree with results from LH run.

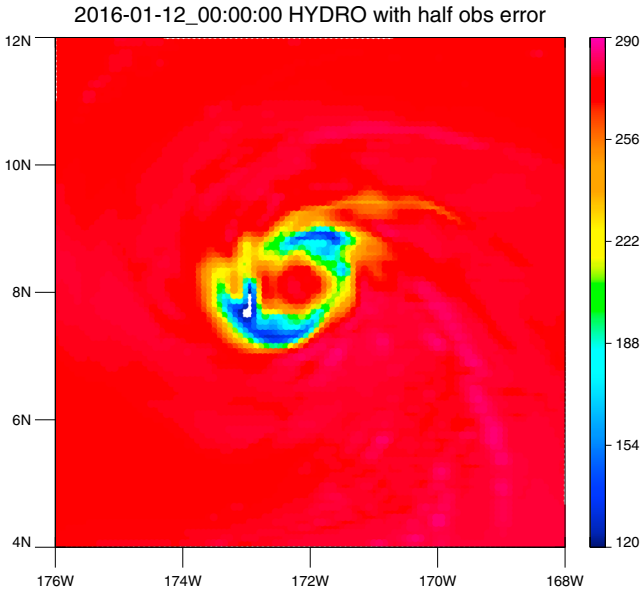

Figure 21. HYDRO run with a decreased observation error by half.

4.3. Impacts of the Observation Error

A key factor that controls the result of the assimilation experiments is the observation error. The forecast error is given by an ensemble forecast, while the observation error is provided by the user depending on observation types and the algorithm used. It ultimately determines how much observation data are allowed in the system. Figure 21 shows a T_b map of a HYDRO experiment in Hurricane Pali's case if a different observation error had been chosen. In this additional DA experiment, the observation error was decreased by 50% or 0.00005 kg/kg. By decreasing the observation error, the system assigns more weight to the assimilated observation than the background data, but assimilates fewer observations because it only allows observations that are similar to the model

background under the same QC ($\frac{|y-\boldsymbol{H}(x)|}{\sqrt{\mathbf{R}}} < \mathbf{3}$) constraint. In Figure 21, the upper rainband, where the difference between the observations and the backgrounds was quite large, is less improved than the previous HYDRO run because most of the observations in that region did not pass the QC. At a minimum, this shows the importance of properly estimating uncertainty in retrieved fields.

5. Conclusions

With an increased number of observations available and various types of DA methods available, it became imperative to find optimal DA frameworks to improve the forecast. T_b and reflectivity have historically been used in clear air condition, but retrieved products are still useful in cloudy and precipitating conditions.

In this study, a method that retrieves three different variables and simultaneously maintains consistency in DSD between observation and forecast model is presented. Microphysical consistency has been ensured by using WRF model outputs to build a retrieval framework. Radar observations are translated into retrieved parameters by searching a database of model fields for which the appropriate reflectivity profile has been computed. With this method, each of three variables (VV, LH, and HYDRO) were retrieved from a single reflectivity profile and assimilated to determine which variable has the most positive impact.

Overall, LH and HYDRO runs provided better results than VV run. This may be due to the weak linkage of a vertical motion to the microphysical scheme. Although it was clear that LH and HYDRO runs were superior to VV run, it is hard to conclude which variable among those two is better. Similar results from LH and HYDRO runs in T_b and reflectivity suggest that the two variables have similar impacts on the DA system. This could have been anticipated because LH and HYDRO are closely related to each other. If computational time is a consideration, LH is preferred as the number of observations for HYDRO was almost twice that for LH. This makes HYDRO computationally more expensive than LH.

These results suggest that even though the same observation is used, its assimilation impacts can vary significantly depending on how the data are processed. Study on the most efficient way of converting raw observation data into useful variables in an assimilation system needs to be investigated further.

Acknowledgments
This research was supported by NOAA's Sandy Supplemental Award NA14OAR4830122. The GFS data were obtained from NOAA National Operational Model Archive and Distribution System (http://nomads.ncdc.noaa.gov/data.php). The 2ADPR data from the GPM satellite were provided by the PPS team at NASA Goddard Space Flight Center, Greenbelt, MD, and can be found at ftp://arthurhou.pps.eosdis.nasa.gov/. The ATCF database is available at ftp://ftp.nhc.noaa.gov/atcf/.

References

Anisetty, S. P. R., Huang, C.-Y., & Chen, S.-Y. (2014). Impact of FORMOSAT-3/COSMIC radio occultation data on the prediction of super cyclone Gonu (2007): A case study. *Natural Hazards*, *70*(2), 1209–1230. https://doi.org/10.1007/s11069-013-0870-0

Atlas, D., Ulbrich, C. W., Marks, F. D., Black, R. A., Amitai, E., Willis, P. T., & Samsury, C. E. (2000). Partitioning tropical oceanic convective and stratiform rains by draft strength. *Journal of Geophysical Research*, *105*(D2), 2259–2267. https://doi.org/10.1029/1999JD901009

Benedetti, A., & Janisková, M. (2008). Assimilation of MODIS cloud optical depths in the ECMWF model. *Monthly Weather Review*, *136*(5), 1727–1746. https://doi.org/10.1175/2007MWR2240.1

Benjamin, S. G., Weygandt, S. S., Brown, J. M., Hu, M., Alexander, C. R., Smirnova, T. G., … Manikin, G. S. (2016). A North American hourly assimilation and model forecast cycle: The rapid refresh. *Monthly Weather Review*, *144*(4), 1669–1694. https://doi.org/10.1175/MWR-D-15-0242.1

Bormann, N., Geer, A., & English, S. (2012). Evaluation of the microwave ocean surface emmisivity model FASTEM-5 in the IFS. European Centre for Medium-Range Weather Forecasts.

Chen, Y., Wang, H., Min, J., Huang, X., Minnis, P., Zhang, R., … Palikouda, R. (2015). Variational assimilation of cloud liquid/ice water path and its impact on NWP. *Journal of Applied Meteorology and Climatology*, *54*(8), 1809–1825. https://doi.org/10.1175/JAMC-D-14-0243.1

Climate Council of Australia (2017). Cranking up the intensity: Climate change and extreme weather events. Retrieved from http://apo.org.au/system/files/73419/apo-nid73419-7336.pdf

Derber, J. C., & Wu, W. S. (1998). The use of TOVS cloud-cleared radiances in the NCEP SSI analysis system. *Monthly Weather Review*, *126*(8), 2287–2299. https://doi.org/10.1175/1520-0493(1998)126%3C2287:TUOTCC%3E2.0.CO;2

Errico, R. M., Bauer, P., & Mahfouf, J. F. (2007). Issues regarding the assimilation of cloud and precipitation data. *Journal of the Atmospheric Sciences*, *64*(11), 3785–3798. https://doi.org/10.1175/2006JAS2044.1

Gallus, W. A. Jr., & Pfeifer, M. (2008). Intercomparison of simulations using 5 WRF microphysical schemes with dual-polarization data for a German squall line. *Advances in Geosciences*, *16*, 109–116. https://doi.org/10.5194/adgeo-16-109-2008

Geer, A. J., & Bauer, P. (2010). Enhanced use of all-sky microwave observations sensitive to water vapour, cloud and precipitation. European Centre for Medium-Range Weather Forecasts.

Geer, A. J., Bauer, P., & Lopez, P. (2010). Direct 4D-Var assimilation of all-sky radiances. Part II: Assessment. *Quarterly Journal of the Royal Meteorological Society*, *136*(652), 1886–1905. https://doi.org/10.1002/qj.681

Han, M., Braun, S. A., Matsui, T., & Williams, C. R. (2013). Evaluation of cloud microphysics schemes in simulations of a winter storm using radar and radiometer measurements. *Journal of Geophysical Research: Atmospheres*, *118*, 1401–1419. https://doi.org/10.1002/jgrd.50115

Hou, A. Y., Kakar, R. K., Neeck, S., Azarbarzin, A. A., Kummerow, C. D., Kojima, M., … Iguchi, T. (2014). The global precipitation measurement mission. *Bulletin of the American Meteorological Society*, *95*(5), 701–722. https://doi.org/10.1175/BAMS-D-13-00164.1

Iguchi, T., Seto, S., Meneghini, R., Yoshida, N., Awaka, J., & Kubota, T. (2010). GPM/DPR level-2 algorithm theoretical basis document (Tech. Rep.). Greenbelt, MD: NASA Goddard Space Flight Center.

Kalnay, E. (2003). *Atmospheric modeling, data assimilation and predictability*. UK: Cambridge University Press.

Kim, J.-H., Shin, D.-B., & Kummerow, C. (2013). Impacts of a priori databases using six WRF microphysics schemes on passive microwave rainfall retrievals. *Journal of Atmospheric and Oceanic Technology*, *30*(10), 2367–2381. https://doi.org/10.1175/JTECH-D-12-00261.1

Kummerow, C. (1993). On the accuracy of the Eddington approximation for radiative transfer in the microwave frequencies. *Journal of Geophysical Research*, *98*(D2), 2757–2765. https://doi.org/10.1029/92JD02472

Kummerow, C. D., Randel, D. L., Kulie, M., Wang, N. Y., Ferraro, R., Joseph Munchak, S., & Petkovic, V. (2015). The evolution of the Goddard profiling algorithm to a fully parametric scheme. *Journal of Atmospheric and Oceanic Technology*, *32*(12), 2265–2280. https://doi.org/10.1175/JTECH-D-15-0039.1

Li, Y., Wang, X., & Xue, M. (2012). Assimilation of radar radial velocity data with the WRF ensemble-3DVAR hybrid system for the prediction of hurricane Ike (2008). *Monthly Weather Review*, *140*(11), 3507–3524. https://doi.org/10.1175/MWR-D-12-00043.1

Lim, K.-S. S., & Hong, S. Y. (2010). Development of an effective double-moment cloud microphysics scheme with prognostic cloud condensation nuclei (CCN) for weather and climate models. *Monthly Weather Review*, *138*(5), 1587–1612. https://doi.org/10.1175/2009MWR2968.1

Ma, Z., Maddy, E. S., Zhang, B., Zhu, T., & Boukabara, S. A. (2017). Impact assessment of Himawari-8 AHI data assimilation in NCEP GDAS/GFS with GSI. *Journal of Atmospheric and Oceanic Technology*, *34*(4), 797–815. https://doi.org/10.1175/JTECH-D-16-0136.1

McCumber, M., Tao, W. K., Simpson, J., Penc, R., & Soong, S. T. (1991). Comparison of ice-phase microphysical parameterization schemes using numerical simulations of tropical convection. *Journal of Applied Meteorology*, *30*(7), 985–1004. https://doi.org/10.1175/1520-0450-30.7.985

Okamoto, K., & Derber, J. C. (2006). Assimilation of SSM/I radiances in the NCEP global data assimilation system. *Monthly Weather Review*, *134*(9), 2612–2631. https://doi.org/10.1175/MWR3205.1

Olson, W. S., Kummerow, C. D., Hong, Y., & Tao, W. K. (1999). Atmospheric latent heating distributions in the tropics derived from satellite passive microwave radiometer measurements. *Journal of Applied Meteorology*, *38*(6), 633–664. https://doi.org/10.1175/1520-0450(1999)038%3C0633:ALHDIT%3E2.0.CO;2

Sampson, C. R., & Schrader, A. J. (2000). The automated tropical cyclone forecasting system (version 3.2). *Bulletin of the American Meteorological Society*, *81*(6), 1231–1240. https://doi.org/10.1175/1520-0477(2000)081%3C1231:TATCFS%3E2.3.CO;2

Shige, S., Takayabu, Y. N., Tao, W. K., & Johnson, D. E. (2004). Spectral retrieval of latent heating profiles from TRMM PR data. Part I: Development of a model-based algorithm. *Journal of Applied Meteorology*, *43*(8), 1095–1113. https://doi.org/10.1175/1520-0450(2004)043%3C1095:SROLHP%3E2.0.CO;2

Skamarock, W. C., Klemp, J. B., Dudhia, J., Gill, D. O., Barker, D. M., Duda, M. G., … Powers, J. G. (2008). A description of the Advanced Research WRF Version 3, NCAR technical note, mesoscale and microscale meteorology division. Boulder, CO: National Center for Atmospheric Research.

Sui, C. H., Tsay, C. T., & Li, X. (2007). Convective–stratiform rainfall separation by cloud content. *Journal of Geophysical Research: Atmospheres*, *112*, D14213. https://doi.org/10.1029/2006JD008082

Tao, W. K., Lang, S., Simpson, J., & Adler, R. (1993). Retrieval algorithms for estimating the vertical profiles of latent heat release. *Journal of the Meteorological Society of Japan Series II*, *71*(6), 685–700.

Wu, T. C., & Zupanski, M. (2017). Assimilating GPM hydrometeor retrievals in HWRF: Choice of observation operators. *Atmospheric Science Letters*, *18*(6), 238–245. https://doi.org/10.1002/asl.748

Wu, T. C., Zupanski, M., Grasso, L. D., Brown, P. J., Kummerow, C. D., & Knaff, J. A. (2016). The GSI capability to assimilate TRMM and GPM hydrometeor retrievals in HWRF. *Quarterly Journal of the Royal Meteorological Society*, *142*(700), 2768–2787. https://doi.org/10.1002/qj.2867

Yang, C., Liu, Z., Bresch, J., Rizvi, S. R., Huang, X. Y., & Min, J. (2016). AMSR2 all-sky radiance assimilation and its impact on the analysis and forecast of Hurricane Sandy with a limited-area data assimilation system. *Tellus A: Dynamic Meteorology and Oceanography*, *68*(1), 30,917. https://doi.org/10.3402/tellusa.v68.30917

Zhang, M., Zupanski, M., Kim, M. J., & Knaff, J. A. (2013). Assimilating AMSU-A radiances in the TC core area with NOAA operational HWRF (2011) and a hybrid data assimilation system: Danielle (2010). *Monthly Weather Review*, *141*(11), 3889–3907. https://doi.org/10.1175/MWR-D-12-00340.1

Zhang, S. Q., Zupanski, M., Hou, A. Y., Lin, X., & Cheung, S. H. (2013). Assimilation of precipitation-affected radiances in a cloud-resolving WRF ensemble data assimilation system. *Monthly Weather Review*, *141*(2), 754–772. https://doi.org/10.1175/MWR-D-12-00055.1

Zhu, Y., Liu, E., Mahajan, R., Thomas, C., Groff, D., Van Delst, P., … Derber, J. C. (2016). All-sky microwave radiance assimilation in NCEP's GSI analysis system. *Monthly Weather Review*, *144*(12), 4709–4735. https://doi.org/10.1175/MWR-D-15-0445.1

Zupanski, M. (1993). Regional four-dimensional variational data assimilation in a quasi-operational forecasting environment. *Monthly Weather Review*, *121*(8), 2396–2408. https://doi.org/10.1175/1520-0493(1993)121%3C2396:RFDVDA%3E2.0.CO;2

Zupanski, M. (2005). Maximum likelihood ensemble filter: Theoretical aspects. *Monthly Weather Review*, *133*(6), 1710–1726. https://doi.org/10.1175/MWR2946.1

Zupanski, M., Navon, I. M., & Zupanski, D. (2008). The maximum likelihood ensemble filter as a non-differentiable minimization algorithm. *Quarterly Journal of the Royal Meteorological Society*, *134*(633), 1039–1050. https://doi.org/10.1002/qj.251